Using relations between stress and fluid pressure for improved compaction modelling in flow simulation and increased efficiency in coupled rock mechanics simulation

Øystein Pettersen
Centre for Integrated Petroleum Research, PO Box 7800, NO-5020 Bergen, Norway

ABSTRACT: The conventional compaction model used in reservoir simulators defines compaction as a function of fluid pressure, whereas, in reality, it is a function of effective stress. The interrelationship between fluid pressure, effective stress and reservoir parameters (materials distribution, geometry, production scheme) is investigated. By modifying the conventional concept of flow simulator compaction a predictor is constructed for the rock mechanics computations in a coupled flow–rock mechanics simulation. This predictor reduces the time to converge the stress computations by reducing or eliminating the number of pore volume iterations in the coupling scheme. Overall computing time is thereby reduced considerably, while maintaining accuracy in the stress computations. Additionally, the compaction state in the flow simulator will be more accurate than in a conventional iterative coupling scheme.

KEYWORDS: *compaction, reservoir simulation, rock mechanics, coupled simulation, effective stress*

INTRODUCTION

A producing reservoir will be influenced by soil compaction in several ways, e.g. in a depletion process the total available compaction energy will govern reservoir pressure development and thereby production rates and totals.

Conventionally, compaction in a reservoir simulator is modelled as a grid cell pore volume multiplier vs. fluid pressure. This is a simplified model used because fluid pressure is the only available parameter for compaction computations in the simulator, and is based only partly on physics, since it does not take account of the reservoir rock behaviour, which may be nonlinear poro-elasto-plastic, depending on stress path, temperature and, possibly, water content (Longuemare *et al.* 2002).

Volumetric compaction is a function of effective stress σ, defined as $\sigma = \sigma_T - \alpha p_f$, where σ_T is total stress, p_f is fluid pressure and α is Biot's constant, which is a measure of the relative significance of grain compressibility versus bulk compressibility (Wood 1990). For incompressible grains α=1; in general $0 < \alpha \leq 1$ (Biot 1941; Terzaghi 1943). Of special relevance for compaction calculations is the mean effective stress p (the average of the diagonal elements in the stress tensor),

$$p = (\sigma_{xx} + \sigma_{yy} + \sigma_{zz})/3, \quad (1)$$

and the volumetric strain ε_p (the sum of the diagonal elements in the strain tensor),

$$\varepsilon_p = \varepsilon_{xx} + \varepsilon_{yy} + \varepsilon_{zz}. \quad (2)$$

During the last decades there has been a growing awareness that the dynamic stress state in the reservoir often has a significant impact on petrophysics and fluid production, and that this interaction can be understood only by performing coupled rock mechanics and reservoir simulator studies (Koutsabeloulis *et al.* 1994; Settari & Mourits 1994, 1998; Gutierrez & Lewis 1998; Koutsabeloulis & Hope 1998; Longuemare *et al.* 2002; Mainguy & Longuemare 2002; Thomas *et al.* 2003). Extending reservoir simulations to also take account of stress state computations will normally increase run time by at least an order of magnitude. Even acknowledging that this is necessary to gain the needed knowledge, there is undoubtedly a need to investigate methods which can reduce overall computing time (e. g. Settari & Walters 1999).

The ideal manner to simulate the soil–fluid interaction is to solve the full coupled system of stress and fluid flow equations (Settari & Walters 1999; Gutierrez *et al.* 2001; Longuemare *et al.* 2002; Lewis *et al.* 2003). This is, however, complex and time consuming. In addition, currently no fully coupled simulator exists, which includes all options provided by the market-leading stress simulators or reservoir simulators, although development of such software is in progress (Koutsabeloulis & Hope 1998; Stone *et al.* 2003; Liu *et al.* 2004) Hence, it is interesting to look at the alternative approach of 'partial coupling', where stress state and reservoir fluid dynamics are computed by dedicated software with data exchange at chosen time steps, called 'stress steps' (Gutierrez & Lewis 1998; Longuemare *et al.* 2002; Mainguy & Longuemare 2002; Dean *et al.* 2003; Thomas *et al.* 2003). In 'explicit' coupling the data exchange is one-way only. First, the flow simulator is run at a time interval ending with the stress step. Then the simulated reservoir state (fluid pressure and saturations) is used to initialize the rock mechanics simulator, which computes the stress state at the time. This computed stress state is used to update the flow simulator data further (typically porosity and/or permeability), where the flow simulator progresses the solution in time to the next time step (Heffer *et al.* 1992). The

Petroleum Geoscience, Vol. **14** 2008, pp. 399–409
DOI 10.1144/1354-079308-718

explicit scheme provides a qualitatively correct stress (and compaction) distribution. However, the stress or compaction level need not be correct, due to the inter-dependency between true compaction and the flow simulator computed compaction used to initialize the rock mechanics simulator. Therefore, the explicit scheme has been improved by iteratively updating the flow simulator cell pore volumes by the values calculated by the rock mechanics simulator at the stress step until convergence, 'iterative' coupling (Settari & Walters 1999; Chin *et al.* 2002; Onaisi *et al.* 2002; Tran *et al.* 2004). As noted by Settari & Walters (1999), iterative coupling is as accurate as full coupling if taken to full convergence, but can be very costly in terms of computing time.

PRELIMINARIES

This paper will investigate the relationship between the true compaction values computed from strain and those computed from fluid pressure, and demonstrate how the flow simulator pore volume compressibility concept can be modified such that the number of iterations in an iterative scheme can be reduced greatly, hence reducing overall processor time considerably.

Some of the referred coupling schemes are based on code modification in the flow simulator and/or the stress simulator, and some are restricted in the choice of poro-elasto-plastic model (e.g. linear elastic). The presented scheme is valid for a general poro-elasto-plastic model and is based purely on data exchange between commercial simulators (no code modification is needed).

The simulators used in the study are the finite-element rock mechanics simulator VISAGE™ from VIPS Ltd (now Schlumberger) (VIPS 2003) coupled to the finite difference reservoir simulator ECLIPSE™ from Schlumberger (Schlumberger 2005). (VISAGE is the mark of VIPS Ltd; ECLIPSE is the mark of Schlumberger.)

The study will use m, the ratio of current to initial cell pore volumes (denoted 'pore volume multiplier'), as a measure of compaction, hence $m = V(t) \,/\, V_0$, where V_0 is the initial pore volume and $V(t)$ the volume at time t.

The flow simulator computes compaction from functions (normally tables) of pore volume multipliers vs. fluid pressure, while, in reality, m is a function of mean effective stress p. Further, for a deforming soil, the compaction of a control volume can be computed from volumetric strain. (The term soil is used, as in Wood (1990) to denote a 'granular material in which significant and often irreversible changes in volume can occur by deformation'. The most relevant examples are sandstones, sands and carbonates such as chalk.)

To distinguish between the different sources for the pore volume multipliers used in the paper, the following notation needs defining:

m_{pf} function of fluid pressure used by flow simulator;

m_p function of mean effective stress;

m_ε computed from volumetric strain, $m_\varepsilon = \exp\left(\varepsilon_p^0 - \varepsilon_p(t)\right)$, where ε_p^0 and $\varepsilon_p(t)$ are volumetric strains initially (no load) and at time t (compressive strain positive).

Provided calculated strains are correct, this m-function represents the true compaction to which other values will be compared.

The notation m_{pf} will be used to denote both the function (table) used for flow simulation, and for grid cell values of m derived from this function (similar for m_p).

The function $m_p(p)$ can be the result of laboratory experiments, but can also be derived from the poro-elasto-plastic model. As shown in Pettersen (2007*b*), Critical State Theory (CST) is the appropriate model for sands or sandstone (or, in practice, a special case of CST, the Cam Clay model (Wood 1990)). For consistency reasons, the $m_p(p)$ used in the simulations were derived directly from the Cam Clay model (Pettersen 2007*b*), or from an extension of CST to chalk.

In order to be consistent with the poro-elasto-plastic model and applicable in the proposed procedure, the flow simulator compressibility function m_{pf} must fulfil some minimum requirements. (1) It must be possible to differentiate the behaviour of m_{pf} during loading and unloading, as, for example, by reversible or irreversible compaction, or partly irreversible (hysteresis). (2) The simulator must allow for multiple functions m_{pf}, valid for different material types defined on separate material regions.

When discussing compaction energy (p_f or p) or compaction, the term 'level' will be used to denote an absolute value of the magnitude (as, for example, the average cell value) and the term 'distribution' to denote (in a non-strict fashion) how the parameter varies in the reservoir. Obviously the reservoir energy or compaction state is correct if – and only if – both level and distribution are correct.

With this notation the iterative scheme can be characterized in the following manner: after a stress step, m_{pf} is set equal to m_ε (calculated by the stress simulator) in all grid cells, and the cycle 'flow simulation–stress simulation–pore volume update' is repeated until $m_{pf} \approx m_\varepsilon$ everywhere. Since changing pore volumes in the flow simulator results in an altered fluid pressure field, the calculated m_ε will also change, which explains why the convergence is often slow. Clearly, the convergence will be much faster if the flow simulator computed pressure and compaction state approximates the true state computed by the stress simulator. The motivation for the procedure presented in this paper is, therefore, to improve the compaction/pressure state used as initializer for the stress computations, which is done by modifying and extending the flow simulator compressibility functions to include a spatial dependency that honours the true space variation as computed by the stress simulator.

SIMPLE SINGLE-MATERIAL TEST CASE

This paper focuses on describing the methodology to derive modified material regions and associated compaction relationships. For clarity of presentation, therefore, a simple test case is used, where interrelations and results can be identified and analysed readily. Obviously, more complex and realistic problems will require a more sophisticated approach, primarily accounting for internal boundary conditions and material-to-material interaction. Some necessary modifications will be discussed briefly, without going into details which only complicate the description.

The test case from which results are presented is a single-material weak sandstone reservoir model, embedded in a relatively stiff surrounding rock, where the outer edge of this rock is constrained from movement. The reservoir soil is isotropic and homogeneous, with porosity 0.3 and horizontal and vertical permeabilities of 3000 mD and 200 mD, respectively. Rock parameters are defined in Table 1.

The Cam Clay model used for the reservoir soil has an initial ellipsis of failure, with major axis equal to the mean effective stress, and horizontal unloading–reloading lines. This is a model for a material that experiences plastic failure with permanent deformation immediately on load, and no recovery on subsequent unloading, which is a realistic model for many sands. (For

Table 1. *Rock parameters for the simple test case*

	Surrounding rock	Reservoir soil
Young's modulus, E	35 GPa	32 MPa
Poisson's ratio, ν	0.19	0.18
Failure model	Mohr-Coulomb	Cam Clay
Cohesion, S_0	24.4 MPa	—
Friction angle, ϕ	30°	20°
Dilation angle, ψ	5°	–
Hardening parameter, H	—	29.5

details on the material model, including the hardening parameter, see Pettersen (2007*b*).)

Grid dimensions

The entire model consists of 78 × 33 × 17 Cartesian elements, of which the outer four rows/layers are used for overburdens, underburdens and side-burdens. Element thicknesses for the overburden are 2500 m, 1000 m, 500 m and 250 m (surface to reservoir) and, for the underburden, 50 m, 200 m, 400 m and 800 m. The side-burdens have element lengths outward from the reservoir 250 m, 500 m, 1000 m and 2500 m. All reservoir elements are 100 × 100 × 5 m. In total, the reservoir proper is 7000 × 2700 × 45 m, while the model including the surrounding rock is 15 500 × 12 200 × 2845 m. Note that the volume of the side-burdens is somewhat smaller than typically used in these kinds of studies, but should be sufficient due to the large contrast in stiffness between the surrounding rock and the reservoir.

Injection/production balance

The reservoir is depleted by five producing wells along the eastern edge (shown by 'up-arrows' in the illustrations) and five injectors along the western edge ('down-arrows'). Well producing liquid target rate is 1200 Sm^3/d, with water injection target rate 600 Sm^3/d.

This gives a depletion rate (average reservoir pressure drop) of approximately 5 bars/year during the first four years (before gas liberation), increasing to a total pressure drop of about 180 bars after 12 years.

FLUID PRESSURE AND MEAN EFFECTIVE STRESS

In a coupled simulation model large volumes of overburden, underburden and side-burdens are included, as in the test example description above. Thus, the interaction between porous and non-porous rock is honoured by the influence of the surrounding soil on reservoir deformation. It is well known that basing compaction calculations on fluid pressure, as in a flow simulator where this interaction is missing, will be inaccurate. A simple illustrative example is shown in Figures 1 and 2, depicting computed compaction from fluid pressure (Fig. 1) and the corresponding 'correct' distribution, as computed from stress simulator strain (Fig. 2), for the test example. As shown in Figure 3, the vertical displacement at the top of the reservoir is non-uniform (bowl-shaped – 'arching effect') causing a compaction field which cannot be reproduced by the fluid simulator, at least not by a conventional compaction model. Omitting the influence of rock mechanics will also often result in an inaccurately simulated flow pattern, due to permeability reduction in compacted volumes (see Pettersen 2007*b*, for example). For the test example, using the compaction field

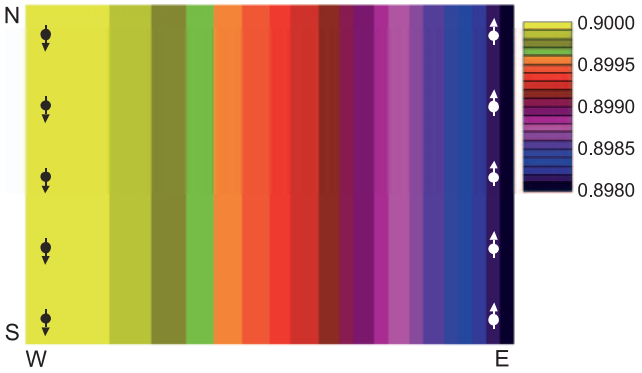

Fig. 1. Isocontours of compaction by conventional fluid simulator model. From the test case, middle reservoir layer at time one year (down-arrows, water injectors; up-arrows, oil producers).

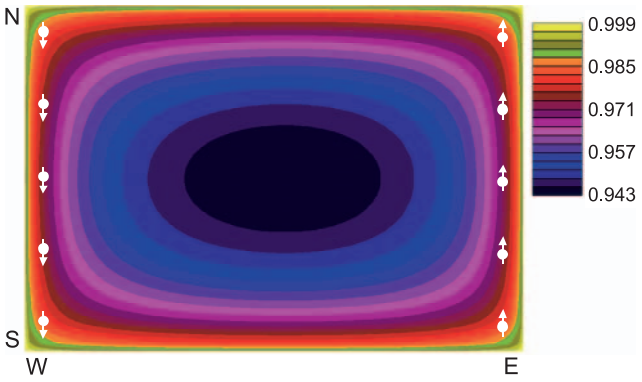

Fig. 2. Isocontours of 'true' compaction, as computed from strain by stress simulator. 'Correct' version of Figure 1. From the test case, middle reservoir layer at time one year.

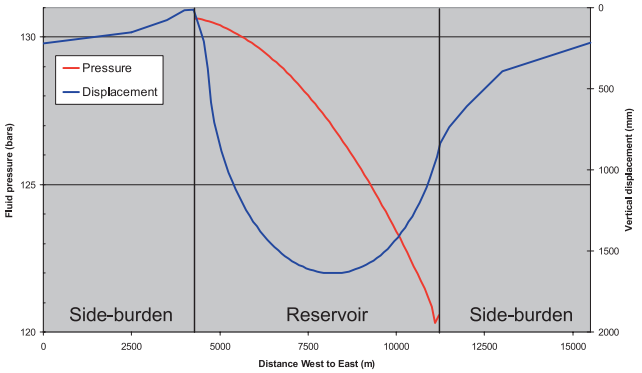

Fig. 3. Total vertical displacement and fluid pressure profile at the top of the reservoir along central W–E axis. From the test case, at time 11 years.

calculated by the flow simulator m_{pf} results in a piston-like fluid front movement (Fig. 4a), while the simulated fluid front shape using the accurate compaction field m_e is as shown in Figure 4b.

For a more realistic example, Figures 5 and 6 show the resulting compaction fields m_{pf} and m_e for a fractured chalk reservoir with several different material types. Although more complex, one can clearly see that the true compaction state is, to a large degree, influenced by material boundary effects, both internal and external. Thus, although a number of parameters contribute to the final stress and compaction state, studies of both simple and complex reservoir models indicate that the difference between m_{pf} and m_e can be explained, largely, by the

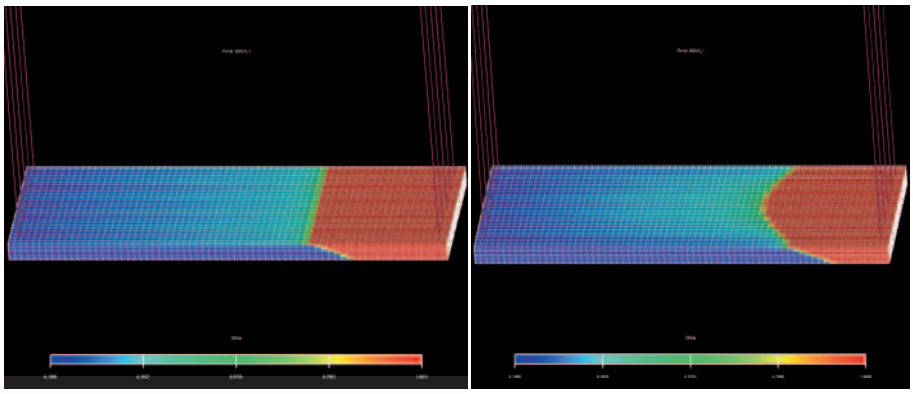

(a) (b)

Fig. 4. Oil saturation profiles for the test case at time six years: (**a**) using 'traditional' compaction model, corresponding to Figure 1; (**b**) using 'correct' compaction as computed by stress simulator, corresponding to Figure 2.

material-to-material interaction, geometry and non-reservoir rock boundary conditions.

MECHANISMS OF COUPLING

Using **x** to denote position (usually grid cell/element), the fluid pressure and compaction state ($p_f(\mathbf{x})$, $m_{pf}(\mathbf{x})$) at a stress step (as exemplified in Fig. 1) is input to, and used as start values for, the stress state computations by the rock mechanics simulator, which calculates the resulting compaction state (as in Fig. 2). This compaction state will be a function of soil properties and the production scheme as discussed above. Many of the qualitative features of the compaction distribution are determined primarily by static soil properties, as the poro-elasto-plastic model, geometry and soil behaviour in the surrounding non-porous rock, defining a quasi-static compaction distribution. On the other hand, the compaction level is determined primarily by the dynamic process, which obviously also influences the distribution; in general, this influence is smaller than the static contribution. Hence, altering m_{pf} will change the flow simulator fluid pressure level and, thus, the choice of m_{pf} has a direct influence on the stress simulator computed compaction level in an explicit scheme. By iterative coupling, the compaction level is then subsequently converged to its correct value. This was also noted by Mainguy & Longuemare (2002) (and others): 'the pore volume compressibility in conventional reservoir simulation is a parameter determined by the reservoir engineer, which can be considered a numerical parameter, since whatever the value supplied by the reservoir engineer, the rock mechanics simulator will provide the exact porosity'. They also demonstrated that the number of iterations needed in an iterative coupling scheme may be very sensitive to this parameter. Apart from this observation, there seems to be no

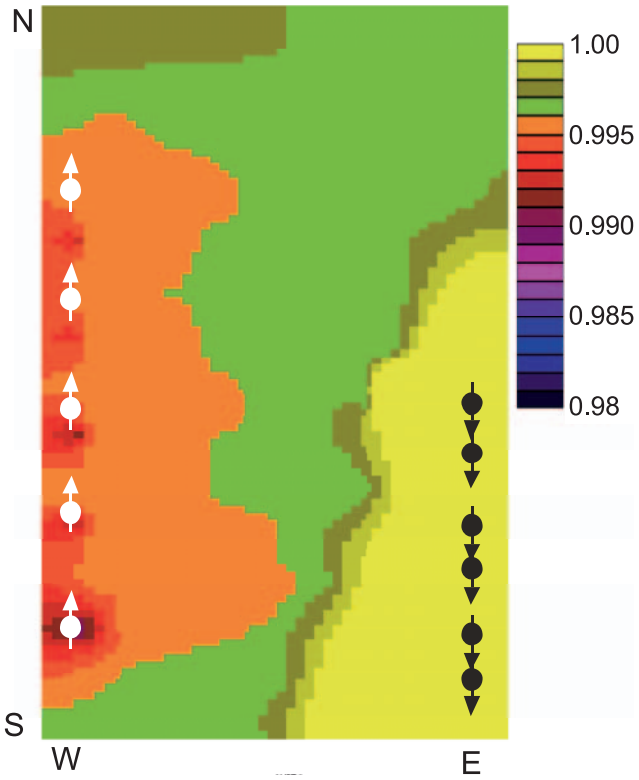

Fig. 5. Isocontours of compaction by conventional fluid simulator model for a more complex rock model, with six anisotropic and heterogeneous materials. From a fractured chalk model, top reservoir layer at time 11 years.

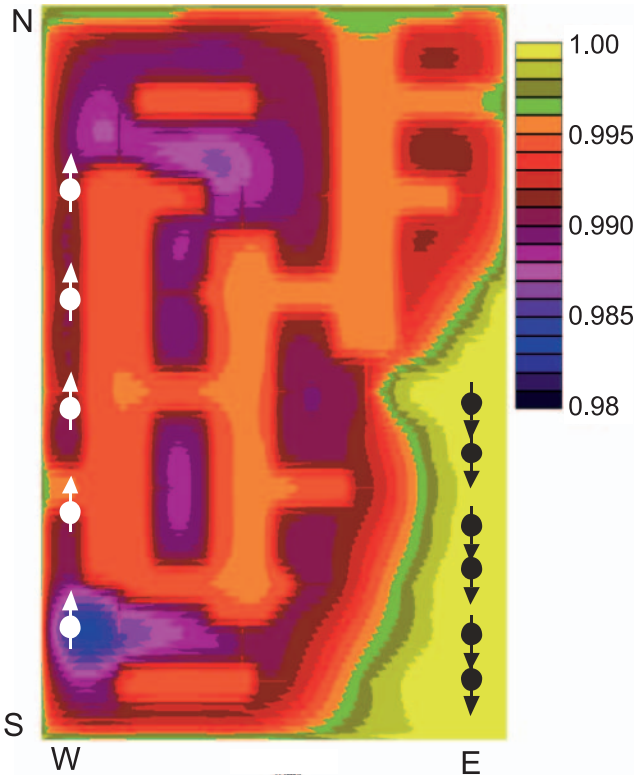

Fig. 6. Isocontours of 'true' compaction, as computed from strain by stress simulator. 'Correct' version of Figure 5. Note how the compaction contours honour the internal boundaries. From a fractured chalk model, top reservoir layer at time 11 years.

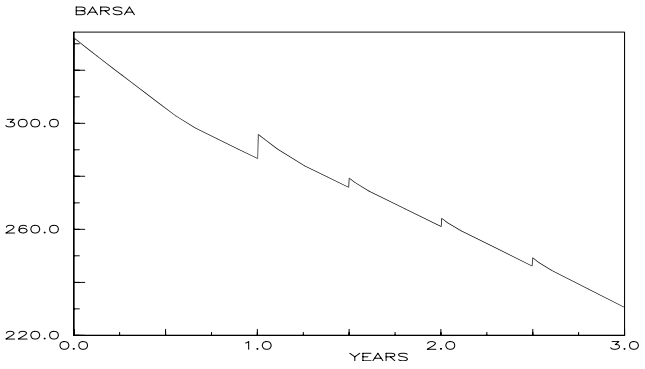

Fig. 7. Average reservoir fluid pressure vs. time, test case with deliberately poor pore volume multiplier tables in the flow simulator, run as an iteratively coupled simulation. The stress steps can be identified easily at the pressure discontinuities, caused by an abrupt change in pore volumes following a pore volume update by the iterative scheme.

attempt to utilize the 'compressibility parameter' to increase the efficiency of coupled simulations in the referred papers.

A first attempt at speeding up the computational scheme could be to try to determine an 'optimal' pore volume compressibility. Since the flow simulator computed compaction distribution is so far from the true distribution, it is, however, not obvious what would be an optimal value, if such a value exists. With this background, it is proposed to extend the conventional concept of pore volume compressibility used by the flow simulator to a compressibility function $m^*_{pf}(\mathbf{x},p_f)$, that, for fixed **x**, will have a pressure dependency determined by scaling of the original $m_p(p)$, and a spatial variation that honours the compaction distribution computed by the stress simulator. Both the level and distribution of this function can be determined from the results of the first (explicit) stress step (as in Fig. 2). If tuned correctly, the compaction state computed by the flow simulator based on $m^*_{pf}(\mathbf{x},p_f)$will be close to the true compaction state, hence the rock mechanics simulations should converge faster, especially with respect to total number of pore volume iterations needed.

Also note that with a conventional iterative scheme, fluid pressures and pore volumes will be correct only at the stress steps, while if the compressibility parameter is inconsistent with the poro-elasto-plastic model, the flow simulator computed pressure development between stress steps will be wrong, with artificial 'adjustment' discontinuities at the stress steps (Fig. 7). This 'feature' can be reduced or removed if the flow simulator uses a pore volume multiplier model, which results in a compaction field closely approximating the stress simulator computed field.

LOCAL BEHAVIOUR – EXTENDED COMPACTION FUNCTIONS

Although no simple relation exists between mean effective stress and fluid pressure, the preceding discussion motivates an assumption that p and p_f can be related locally, i.e. for a fixed position **x**, $p(\mathbf{x})=p(p_f(\mathbf{x}))$. From (iterative) coupled simulations with varying kinds of material data, the behaviour of p versus p_f in single cells has been examined, and it has been found that, in general, the assumed relation does exist, at least approximately. An example is shown in Figure 8. Further, since the loading/unloading characteristics in each grid cell are governed primarily by the local energy change, a predictor for the rock mechanics calculations is proposed.

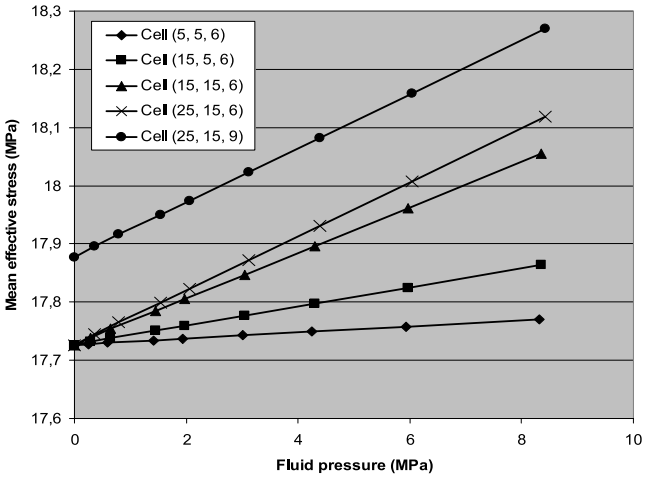

Fig. 8. Mean effective stress vs. depleted pressure for some (single) cells, from the test case. The curves demonstrate a local relationship $p=p(p_f)$.

Predictor – extended compaction functions

Locally, i.e. for a fixed **x**,

i $p(\mathbf{x})=p(p_f,\mathbf{x})$

ii $m^*_{pf}(\mathbf{x},p_f)$is a scaled version of $m_p(p)$.

The novel concept here is that the extended flow simulator compressibility function $m^*_{pf}(\mathbf{x},p_f)$ also honours the spatial variation found by the stress simulator. (Note: the spatial variation captured by the extended compressibility function is for a single material. For multi-material cases, one extended function must be defined for each of the original materials.)

The extended functions should preferably be easy to construct, hence the assumption that for fixed **x**, the function can be found by a simple transformation of $m_p(p)$. Details of this transformation will be given in a later section.

If the predictor is exact, the extended compressibility function can be computed at the first stress step and, thereafter, an accurate compaction state can be computed (by the flow simulator) from the fluid pressure state at all subsequent times, including later stress steps. In each grid cell, the flow simulator computes a pore volume multiplier and fluid pressure from the local compaction relation valid for the cell in question, constructed by the assumption (ii). Then, the corresponding mean effective stress computed from assumption (i) will be in agreement with the rock mechanics simulator computed p and, hence, $m_{pf}=m_e$ in the cell.

Obviously, the predictor will be exact only exceptionally, but, for simple cases, the initial cell m_{pf} computed by the predictor algorithm will often be a good approximation to the actual multiplier and at least significantly better than the conventional flow simulator pore volume multiplier. In general, a dynamic update as described below will be needed to determine a reliable m_{pf}.

When the flow simulator computed compaction state is close to the true state, and this state is used as initializer for the rock mechanics simulator, stress computations will necessarily converge faster. Additionally, since the extended compressibility function is used by the flow simulator for calculations between stress steps, and the compaction state is (almost) correct at the stress steps, fluid pressure and compaction development will be (nearly) correct and continuous at all times.

Fig. 9. Pseudo-material regions generated by the procedure. Test case, middle reservoir layer.

Pseudo-material regions

In practice it is not necessary (or desirable) to use one compressibility function for each grid cell, which would also be memory-requiring for large grids. Instead, each original material region is subdivided into several 'pseudo-material regions', each with its own compaction function, such that all cells in a pseudo-region have almost equal compaction functions, approximated by the common pseudo-region compaction function. The number of such pseudo-regions is determined by an error tolerance. In practice, it has been found that generally no more than 25 pseudo-regions are needed (for each parent region), often fewer. An example is shown in Figures 9 and 10. In the test case there is only one material originally, so the single parent material region comprises the entire reservoir. Ten pseudo-material regions were constructed based on results from the first stress step, and the resulting regions in one reservoir layer are shown in Figure 9. Each of these regions is associated with one extended compaction function $m^*_{pf}(p_f)$, constructed by scaling the original $m_p(p)$. The ten extended compaction functions (vs. fluid pressure) and the original $m_p(p)$ (versus mean effective stress transformed to equivalent pressure) are shown in Figure 10.

These pseudo-material regions and compaction functions were then used in the flow simulator. The flow simulator computed compaction state m_{pf} at a later stress step is shown in

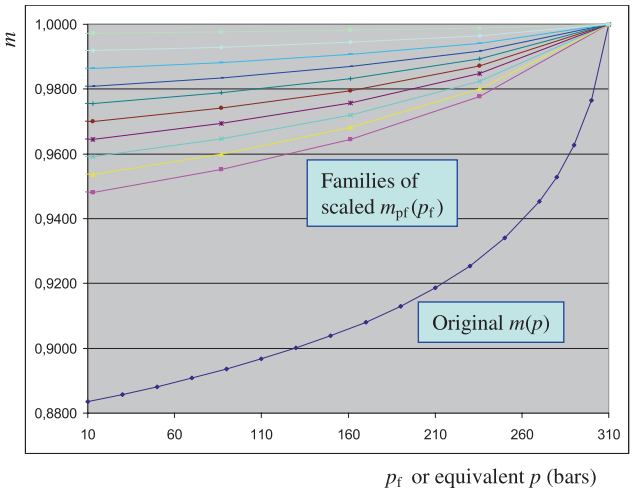

Fig. 10. Extxended compressibility functions associated with the regions in Figure 9, as generated initially by the procedure (no dynamic update). Lower curve in the upper set is for pseudo-region 1 (central part of reservoir), upper curve is for pseudo-region 10.

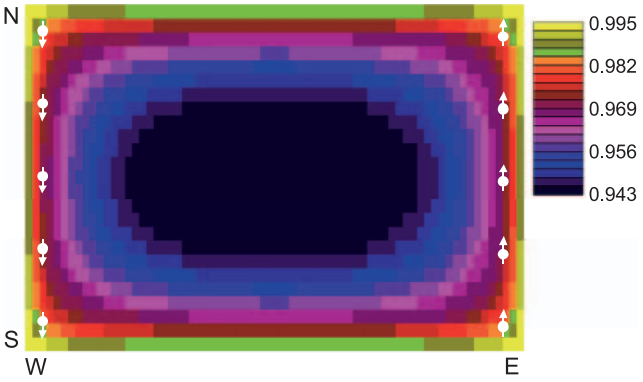

Fig. 11. Isocontours of compaction as computed by the flow simulator using pseudo-material regions and pore volume multiplier tables, as in Figures 9 and 10. Test case, middle reservoir layer at time 11 years.

Figure 11 and the resulting m_ε computed by the rock mechanics simulator in Figure 12. This compaction state has correct level, and was found without iterations. Note that Figures 11 and 12 are not identical, which they would be if the predictor was exact, but the state in Figure 11 is an excellent starting point for the rock mechanics simulator solver.

SCALING

The primary basis for scaling of the compaction functions is correlation plots of m_ε vs. p_f. An example of such a plot is shown in Figure 13, where each point represents the value of m_ε vs. p_f in one grid cell, plotted for all cells. For single-material homogeneous models, such as the test case, the points will typically form bowl-shaped bands, with the points at the base of the bowl corresponding to cells near the middle of the reservoir. Results from six different stress steps are shown in this figure. Intuitively, and confirmed by focusing on chosen cells, the lower envelope of the point cloud is a measure of compaction far from boundaries. The envelope is shown as a red line in Figure 13 and, as it represents the compaction level as a function of fluid pressure, it is denoted the level function, m_1. $m_1(p_f)$ is the basis for the compaction function for the central pseudo-material region, and the other pseudo-compaction functions are constructed simply by scaling of m_1. In Figure 13, the shape of m_1 is apparent since there are results from several stress steps. But this is only for illustrative purposes, as m_1 will be constructed from results at stress step 1. The initial shape of

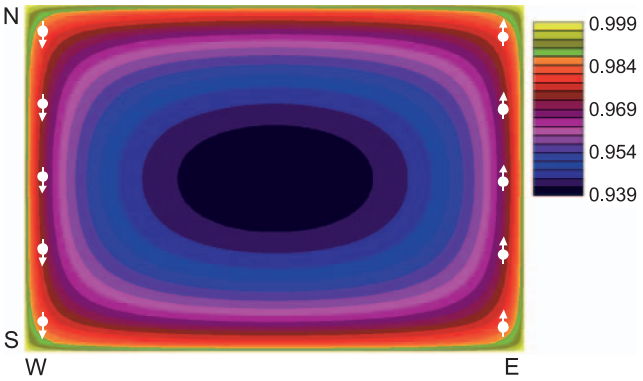

Fig. 12. Isocontours of compaction computed from stress simulator strain in a coupled run. The stress simulator converged without any pore volume iterations when the compaction state from Figure 11 was used as initializer (predictor). Test case, middle reservoir layer at time 11 years.

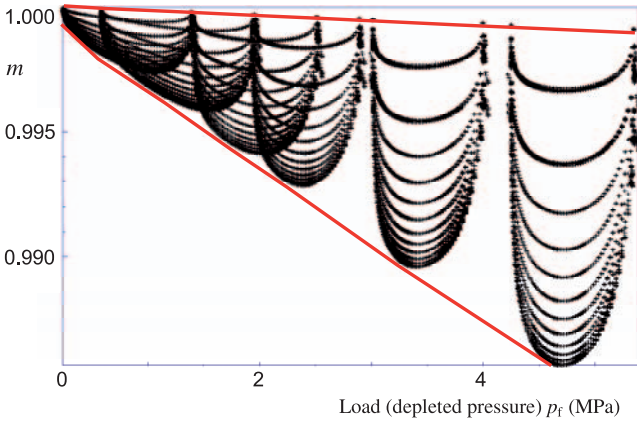

Fig. 13. Correlation plot m_ε vs. p_f. Cell values of p_f and corresponding m_ε are shown for all cells in the reservoir for stress steps 1–6. Lower ('level function') and upper envelopes are shown in red. Test case.

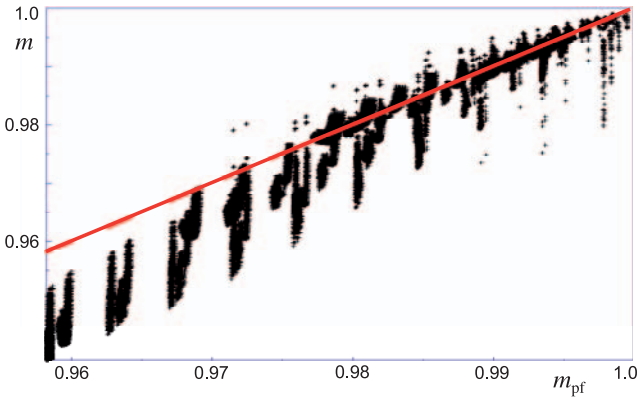

Fig. 14. Correlation of m_ε vs. m_{pf}. Cell value pairs: compaction from the flow simulator model vs. the true compaction value from stress simulator strain at stress steps 1–5. A perfect match is shown by the red line. Test case using pseudo-materials, as in Figures 9 and 10, without dynamic update of pore volume multipliers. This clearly shows how the flow simulator m_{pf} drifts away from the correct curve with time.

the function is then defined by assumption (ii), the transformation $m_p(p) \rightarrow m_1(p_f)$ is shape-conserving. At later stress steps, m_1 is updated and improved as more results become available. Experience shows that only one or two such updates are needed before a reliable compaction function has been derived (note that all the stress simulations are performed in explicit mode, without pore volume iterations).

For multi-material problems, one level function is defined for each original material region and, although a concept such as 'far from boundaries' is no longer necessarily applicable when internal material boundaries and material interaction must be accounted for, the lower envelope will nevertheless be generally well defined. Although more complex to implement, multi-material cases can be handled essentially the same way as single material cases.

The tuning run – determining the level function explicitly

An essential property of the level function $m_1(p_f)$ is that it can be determined by one explicit stress simulator run (or a few if dynamic update is needed), without iterations (the 'tuning run'). This is because, as noted above, irrespective of the initial guess of $m_{pf}(p_f)$, the stress simulator computes the correct stress/strain distribution, primarily dependent on material distribution, properties and boundary conditions. The level function (or, in fact, any of the single-cell compressibility relations) is uniquely defined by the poro-elasto-plastic model, and bears no relation to the compressibility function used in the flow simulator tuning run. This implies that even though a computed cell pressure typically is incorrect, any cell state $(p_f, m_1(p_f))$ found by the tuning run will be a valid combination of fluid pressure and compaction (consistent with the poro-elasto-plastic model). The required point on the level function can then be extracted from the point cloud, after which $m_1(p_f)$ can be constructed.

Obviously, after the extended compressibility function has been constructed, the coupled simulation up to and including the first stress step must be repeated, using the newly defined extended compressibility functions and associated pseudo-material regions in the flow simulator.

Dynamic update of the extended compressibility functions

At the end of each stress step, $m_1(p_f)$ and the associated compaction functions are tested and, if necessary, modified to honour the results from the current stress step, such that the level function at any time is the lower envelope of all available $m_\varepsilon(p_f)$-data, extended to unverified pressure values by transforming the initial shape such that it honours the recorded data. In this manner an accurate relation $m_1(p_f)$ is constructed by the process and can be used, for example, in later simulations for similar problems in the same reservoir, as an optimal predictor. The essential difference between this approach and traditional pore volume iterations is that in lieu of updating each cell's pore volume, the procedure updates the functional relationship $m=m(p_f)$, which can then be used to compute accurate pore volumes and pressures simultaneously.

ERROR ANALYSIS

The quality of the scheme is assessed at the end of each stress step by examining correlation plots of m_ε vs. m_{pf}. Such a plot is shown in Figure 14, where each point represents the value of m_ε vs. m_{pf} in one grid cell. For illustrative purposes the referred simulation was run five stress steps explicitly and without updating the extended compressibility functions. In a 'perfect' run all points would lie on the line $m_\varepsilon=m_{pf}$, shown in red on the figure. Since this is a pure depletion process, the stress steps increase towards the left in the figure (smaller values of the pore volume multiplier). Two different kinds of error growth can be observed in Figure 14: (1) the total error (difference between maximum and minimum of m_ε) increases with increasing time; and (2) the average of m_ε drifts away from the line $m_\varepsilon=m_{pf}$.

The latter effect is a result of an erroneous compaction level and is corrected by the dynamic adjustment of $m_1(p_f)$. The effect of this is demonstrated in Figure 15, where two dynamic updates were performed, after which the rest of the coupled simulation was run in explicit mode. Hence, a total of eight stress simulations were performed, which compares favourably to running the same problem with pore volume iterations, even if only two iterations were needed at each stress step. Experience comes from the pore volume iteration scheme as implemented in Visage, where typically at least three, often more than ten iterations are needed. However, other schemes have been developed, where convergence may be faster.

If the total error grows beyond some prescribed tolerance, the number of pseudo-material regions may be too low, or the

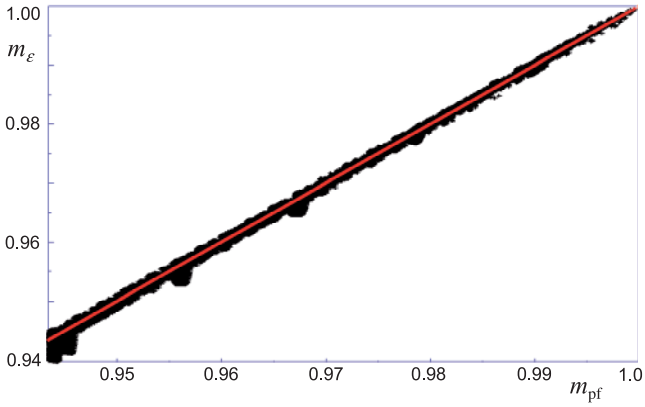

Fig. 15. Correlation of m_ε vs. m_{pf} as in Figure 14, but with dynamic update of the pore volume multiplier tables at stress steps 2 and 5.

initial choice of such regions is no longer valid, which presumably could occur in processes with significantly changing production scenarios. In such cases it would be necessary to redefine the pseudo-material regions and possibly rerun the latest stress step; such an occurrence will increase run times. It should be mentioned that such behaviour has not been observed in any of the cases studied, whether simple or complex. Experience shows that if the number of pseudo-regions is chosen such that the initial error is well within the tolerance to allow for some growth, then redefinition of pseudo-regions is not needed, even for problems with a complex production scenario.

A COMMENT ON COMPOUND SOILS

Although multi-material reservoirs are not discussed elaborately in this paper, an aspect of these should be mentioned. For such cases, the analysis can be more complex, as internal material boundary conditions and material interaction must be accounted for when constructing the pseudo-material regions. The influence of material geometry can seem unpredictable, at times, and intuitively logical initial material region definitions can turn out to be inappropriate. An example of such a case is shown in Figure 16, taken from a study of a fractured chalk reservoir, depicting two distinctly different trends for m_ε vs. p for one of the material regions. The failure model for the chalk

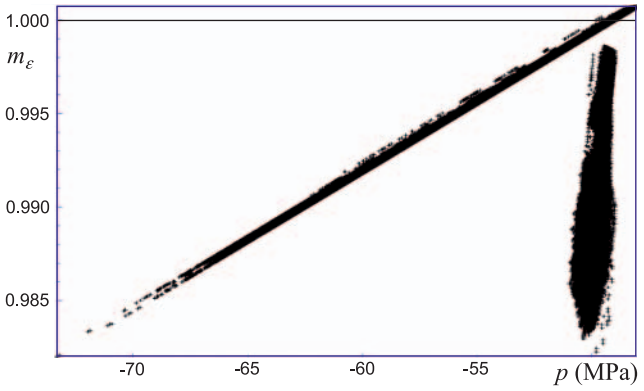

Fig. 16. Correlation of m_ε vs. mean effective stress p for one material (transition matrix ↔ fractures) in the fractured chalk model, stress steps 1–6. The left-hand branch comprises all cells with a distance at most of four grid cells from a fracture, while the right-hand branch comprises cells further away from a fracture. The figure reveals that these cells were assigned to the 'wrong' region and should have been assigned to the matrix material region.

is essentially an extended Cam Clay model, allowing for water weakening and swelling, and more realistic dilation. The material referred to in Figure 16 is the transition zone between chalk matrix and explicitly modelled fractures (Mohr-Coulomb with stress-dependent fracture closure). Material properties for the matrix and transition zone are identical, except that the transition zone includes implicitly modelled fractures. Some key parameters: Young's modulus: 1.5 GPa; Poisson's ratio: 0.18; hardening parameter: 4.4; tensile strength: 0.4 MPa; friction angle: 35°; cohesion: 0.3 MPa.

The functional relationship between compaction and mean effective stress must be considered well established, so the two different branches in Figure 16 must be due to some material interaction mechanism. Searching for a mapping between grid cells and the two branches revealed that all cells that were at most four grid cells away from a fracture belong to the left-hand branch in Figure 16, while all cells that were further away from the fractures belong to the right-hand branch. The trend observed in the right-hand branch also agrees with corresponding results from neighbouring matrix. It is, perhaps, surprising that such a division generates two so distinctly different branches, with no points in between. In this case, the initial definition of the transition zone was obviously too rough and must be redefined to include exactly those cells sufficiently close to a fracture. Although easily fixed, it is an inconvenience that such behaviour cannot always be predicted, and automatic detection and repair is not straightforward to implement. So, although the complete procedure for running reasonable well-behaved cases by the described procedure has been automated, more complex cases still require some reservoir engineering assistance. On the other hand, the benefit in terms of reduced computer time is larger for complex cases, so the time spent is well worth the effort.

An example of how the procedure performs on a realistic and complex example is given in Figure 17, which shows the compaction field as computed from the flow simulator for the fractured chalk problem. The original model's six material regions were subdivided into a total of 135 pseudo-regions by the procedure, using a tuning run with two dynamic updates of the m-functions. The state in Figure 17 should be compared to Figures 5 and 6. The stress simulator compaction from strain shown in Figure 6 was carried out in one explicit run, using the state of Figure 17 as initializer. While Figures 6 and 17 are far from identical, they have many features in common.

The main purpose of the state in Figure 17 was then to provide the stress simulator with an excellent starting point for calculating the accurate stress solution with as little effort as possible. Details of the application of the procedure to the fractured chalk problem can be found in Pettersen (2007*a*).

SOME PRACTICAL CONSIDERATIONS

Although all producing reservoirs will be influenced by rock mechanics to some degree, there are large variations in the kind of stress-dependent behaviour, which motivate different attack angles when performing simulation studies.

For reservoirs containing mainly reasonably strong rock, the influence of rock mechanics on flow will generally be small and, as an example, the spatial variation of compaction discussed in this paper will have little or no effect on the flow pattern. For such reservoirs, the only important issue related to compaction is typically to get the overall level correct, ensuring correct energy balance. This will often be done by history matching, and there is normally no need to do any rock mechanics simulations.

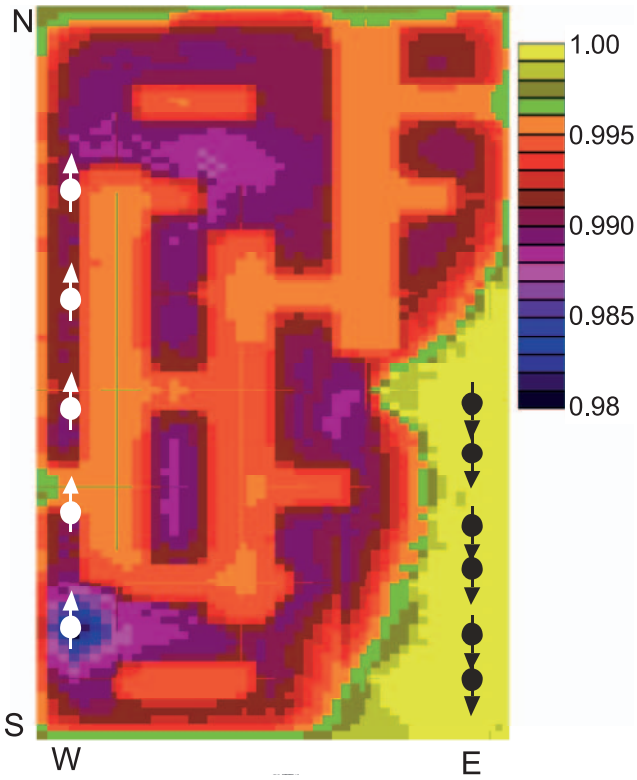

Fig. 17. Isocontours of compaction as computed by the flow simulator using pseudo-material regions and pore volume multiplier tables. The original six reservoir material regions were subdivided into a total of 135 pseudo-regions by the procedure. The associated compaction curves were dynamically updated twice. Fractured chalk model, top reservoir layer at time 11 years. Compare with Figures 5 and 6.

In weaker soils, compaction and spatial variation of compaction may have significant influence on the flow pattern. Further, the soils may depict more complex rock mechanics behaviour, such that rock mechanics simulations are needed to understand both flow and soil-related problems. Examples include subsidence, fracture closure and opening, fault activation and deactivation, dilation and creep. In these cases, the rock mechanics simulations are part of the essential toolbox to gain a full understanding of the production process. Usually many stress step solutions will be needed to achieve this, so reducing the number of stress steps is not an issue. The complex rock mechanics effects will certainly also influence the compaction, and the question is what impact this may have on the computations in the described algorithm.

The main feature of the presented procedure is to provide an improved flow simulator compaction state for use as input to the stress simulator in a coupled simulation. However complex the reservoir soil behaviour may be, for compaction calculation purposes the end result is the strain state computed by the stress simulator. Thus, as long as the computed strains are reliable, in principle the procedure should work irrespective of the complexity of the underlying problem. The simple relation between volumetric strain and compaction is crucial for the procedure in its present state and, if other mechanisms influence compaction such that the relation no longer holds, the algorithm will obviously need a modification to take account of this. Hitherto, only the volumetric strain dependency has been included, but future experience gained from more complex models may motivate further work on this subject.

Also, the derived compaction model must be acceptable by the flow simulator. Partial recovery on unloading, and many unloading–reloading cycles can be incompatible with the flow simulator compaction model, although many such processes can be simulated satisfactorily by irreversible compaction curves, or hysteresis. In the construction algorithm, the unloading–reloading processes were disregarded and only points on the primary loading curves were used. The motive for this approach was mainly practical – typical simulation results will not contain sufficient data for the unloading–reloading behaviour to enable construction of secondary curves for all the pseudo-material regions involved. However, it has been found that 'good enough' hysteresis curves for flow simulator use can be defined by the user, based on percent recovery from experimental or simulated data.

However good the flow simulator compaction model may be, there will always be some geomechanical features that are impossible to include. One example is dilation, whereby local volume increase occurs during loading. Such behaviour is not permitted by the flow simulator and must therefore be computed in the subsequent stress simulation. This is but one example demonstrating that even for pure compaction-related issues, it is not even theoretically possible for the flow simulator model alone to capture all effects.

The bottom line is that provided the strain-based compaction calculations can be trusted, the compaction state computed by the flow simulator using the pseudo-materials concept will be a good approximation to the true compaction state. Although essential features (like dilation) may be lacking, this state will be optimal as initializer for the stress simulator in a coupled scheme, and allows the stress simulator to compute the reservoir stress state to full accuracy without pore volume iterations. The final, explicit stress solution should not lack any information compared to a traditional iterative coupled run, since the stress simulator problem definition remains unaltered, apart from a better starting point. (One can envisage cases where pore volume iterations would still be needed, but in such cases it would still be assumed that the convergence will be faster than by using the traditional initializer.)

For many moderately complex problems where the soil behaviour *per se* is not critical, coupled simulations are often omitted in the reservoir engineering community, although the flow definitely can be influenced by the rock mechanics, as demonstrated by, for example, the simple test case. In some cases a qualitative compaction distribution, as in Figure 11, can be (and has been) manually constructed by defining compaction curves and pore volume multipliers similar to Figures 9 and 10, guided by intuition and history matching data. Although this may work to some extent, in practice, it lacks the physical foundation of the method presented in this paper and is not carried over easily to more complex cases.

Especially when regarding correlation plots, such as in Figure 15, it could be tempting to conclude that the flow simulator results appear to be 'good enough' and thereby skip the stress simulations altogether. Such an approach is, however, not recommended. First, the coupled simulations are needed to establish the quality of the flow simulation and, secondly and more importantly, it has been demonstrated and experienced that the flow simulator will never or seldom be able to capture all the mechanisms that contribute to establishing the true compaction state.

An interesting question regards the robustness of the constructed compaction relationships. Intuitively, one would believe that the curves were related closely to the production process by which they were constructed, such that adding or removing wells, or changing well rates would render the curves invalid. In

practice, it has been found that the curves are surprisingly robust with the respect to the production scenario. An intuitive explanation for this is that when, for example, a producing rate is increased, the ensuing increase in pressure drop is accompanied by a corresponding change in mean effective stress and, if the local p_f vs. p relation is valid at the new pressure values, the correct change in compaction will be captured.

In conclusion, the procedure will improve work flow for all kinds of problems where coupled runs are needed. When flow simulator results are the main objective, the number of stress steps can often be reduced compared to traditional coupled simulation with pore volume iterations. For problems where the stress simulations are the main objective, and the flow simulations serve primarily as input to the stress simulations, the main advantage is the elimination (or reduction) of pore volume iterations. Regardless of the problem type, the stress simulator results will be of no lower quality than using the alternative scheme, but generally can be achieved faster, since the total number of pore volume iterations will be lower – often considerably lower. Also, one should not underestimate the value of uniformly accurate flow simulator results, as opposed to results that are reliable only at the stress steps.

COMPUTER PERFORMANCE – EXPERIENCE

The procedure requires one, or a few additional (explicit) stress simulations, the tuning run. For the remaining stress steps, only exceptionally will more than the one explicit stress simulation be needed. Hence, most of the hard work is done in the tuning run; later stress steps will require the processor time as for explicit coupling. A number of cases have been run with varying material definitions, both single material and multi-material problems. For testing purposes all runs were set up as iteratively coupled, but in no cases were more than one iteration needed at any stress step.

Experience with respect to computing time is, therefore, that pore volume iterations are eliminated in general, which in the extreme can reduce total computing time by more than 90% (as compared to the Visage pore volume iteration scheme).

CONCLUSIONS

The compaction state computed by a flow simulator (based on fluid pressure) is very different from the actual compaction state calculated from strain, which in many cases will result in an erroneous fluid flow pattern if simulated by a flow simulator alone. This will be especially relevant for reservoirs containing weak sands or many chalk reservoirs. Further, due to this large difference, the flow simulator calculated compaction state is typically not a good initializer for the stress calculations. By extending the conventional concept of flow simulator compaction functions to functions that are also space- and time-dependent, and optimizing these by the stress simulator results, significantly more accurate compaction calculations are obtained from the flow simulator. These act as an excellent predictor for the rock mechanics simulator calculations, which normally can then be performed explicitly (no iterations) with the same accuracy as a traditional iterative coupled simulation, hence reducing processor time for this simulator considerably. The high quality of the flow simulator computed compaction, in many cases, also allows for fewer stress steps in a coupled simulation, so the overall gain can be twofold.

The author would like to thank BP/Valhall for funding and support to this work, and VIPS Ltd (now Schlumberger) for support and helpful discussions.

REFERENCES

Biot, M.A. 1941. General theory of three dimensional consolidation. *Journal of Applied Physics*, **12**, 155–163.

Chin, L.Y., Thomas, L.K., Sylte, J.E. & Pierson, R.G. 2002. Iterative coupled analysis of geomechanics and fluid flow for rock compaction in reservoir simulation. *Oil, Gas Science and Technology – Rev. IFP*, **57**, 485–497.

Dean, R.H., Gai, X., Stone, C.M. & Minkoff, S.E. 2003. A comparison of techniques for coupling porous flow and geomechanics. Paper SPE 79709 presented at the SPE Reservoir Simulation Symposium, 3–5 February, Houston, Texas.

Gutierrez, M. & Lewis, R.W. 1998. The role of geomechanics in reservoir simulation. Paper SPE/IRSM 47392 *In: Proceedings of Eurock 98*, 8–10 July, Trondheim, Norway, **Vol. 2**, 439–448.

Gutierrez, M., Lewis, R.W. & Masters, I. 2001. Petroleum reservoir simulation coupling fluid flow and geomechanics. *SPE Reservoir Evaluation & Engineering*, **4**(3), 164–172 (SPE72095 PA).

Heffer, K.J., Last, N.C., Koutsabeloulis, N.C. & Chan, M. 1992. The influence of natural fractures, faults and earth stresses on reservoir performance – analysis by numerical modeling. Paper presented at the 3rd International Conference on North Sea Oil and Gas Reservoirs, November, Trondheim, Norway.

Koutsabeloulis, N.C. & Hope, S.A. 1998. 'Coupled' stress/fluid/thermal multi-phase reservoir simulation studies incorporating rock mechanics. Paper SPE/IRSM 47393 *In: Proceedings of Eurock 98*, 8–10 July, Trondheim, Norway, **Vol. 2**, 449–454.

Koutsabeloulis, N.C., Heffer, K.J. & Wong, S. 1994. Numerical geomechanics in reservoir engineering. *In:* Siriwardane, H. & Zeman, M. (eds) *Computational Methods and Advances in Geomechanics*. Balkema, Rotterdam, 2097–2104.

Liu, Q., Stone, T., Han, G., Marsden, R. & Shaw, G. 2004. Coupled stress and fluid flow using a finite element method in a commercial reservoir simulator. Paper SPE 88616 presented at the SPE Asia Pacific Oil and Gas Conference and Exhibition, 18–20 October, Perth, Australia.

Lewis, R.W., Makurat, A. & Pao, W.K.S. 2003. Fully coupled modeling of seabed subsidence and reservoir compaction of North Sea oil fields. *Hydrogeology Journal*, **11**, 142–161.

Longuemare, P., Mainguy, M., Lemonier, P., Onaisi, A., Gérard, Ch. & Koutsabeloulis, N. 2002. Geomechanics in reservoir simulation: overview of coupling methods and field case study. *Oil & Gas Science and Technology – Rev. IFP*, **57**, 471–483.

Mainguy, M. & Longuemare, P. 2002. Coupling fluid flow and rock mechanics: formulations of the partial coupling between reservoir and geomechanical simulators. *Oil & Gas Science and Technology – Rev. IFP*, **57**, 355–367.

Onaisi, A., Samier, P., Koutsabeloulis, N.C. & Longuemare, P. 2002. Management of stress sensitive reservoirs using two coupled stress-reservoir simulation tools: ECL2VIS and ATH2VIS. Paper SPE 78512, 10, presented at the Abu Dhabi International Petroleum Exhibition and Conference, 13–16 October.

Pettersen, Ø. 2007*a*. An improved compaction model for reservoir simulation and coupled flow–stress simulation. Report UP 05/2007. Unifob AS, University of Bergen.

Pettersen, Ø. 2007*b*. Sandstone compaction, grain packing and critical state theory. *Petroleum Geoscience*, **13**, 63–67.

Schlumberger. 2005. *ECLIPSE Reference Manual*. Schlumberger Information Solutions, Houston, Texas.

Settari, A. & Mourits, F.M. 1994. Coupling of geomechanics and reservoir simulation models. *In:* Siriwardane, H. & Zeman, M. (eds) *Computational Methods and Advances in Geomechanics*. Balkema, Rotterdam, 2151–2158.

Settari, A. & Mourits, F.M. 1998. A coupled reservoir and geomechanical modeling system. *SPE Journal*, **3**(3), 219–226 (SPE50939 PA).

Settari, A. & Walters, D.A. 1999. Advances in coupled geomechanical and reservoir modeling with applications to reservoir compaction. Paper SPE 51927, presented at the SPE Reservoir Simulation Symposium, 14–17 February, Houston, Texas.

Stone, T.W., Xian, C., Fang, Z., Manalac, E., Marsden, R. & Fuller, J. 2003. Coupled geomechanical simulation of stress dependent reservoirs. Paper SPE 79697 presented at the SPE Reservoir Simulation Symposium, 3–5 February, Houston, Texas, USA.

Terzaghi, K. 1943. *Theoretical Soil Mechanics*. Wiley, New York.

Thomas, L.K., Chin, L.Y., Pierson, R.G. & Sylte, J.E. 2003. Integrating geomechanics in full-field 3-D reservoir simulation – modeling techniques and field applications. Paper SPE 77724, presented at the SPE Applied Technology Workshop, 31 July–1 August, Corpus Christi, Texas.

Tran, D., Settari, A. & Nghiem, L. 2004. New iterative coupling between a reservoir simulator and a geomechanics module. Paper SPE 88989, *SPE Journal*, **9**(3), 362–369 (SPE88989 PA).

VIPS. *The VISAGETM System User's Guide*. VIPS Ltd, Bracknell.

Wood, D.M. 1990. *Soil Behaviour and Critical State Soil Mechanics*. Cambridge University Press, Cambridge, UK.

Received 30 May 2006; revised typescript accepted 17 January 2008.